The effect of end walls on subcritical flow between concentric and eccentric rotating cylinders

M. J. El-Dujaily
Mathematics and Statistics Department, Polytechnic South West, Plymouth PL4 8AA, UK

F. R. Mobbs
Mechanical Engineering Department, University of Leeds, Leeds LS2 9JT, UK

Visual observations and numerical solutions of the flow equations have been used to study the flow between a rotating inner cylinder and a stationary outer cylinder. The annulus length is defined by stationary end walls and both concentric and eccentric cylinders are considered at Taylor numbers below the critical value.

The numerical results show vortex motions to be present at very low subcritical Taylor numbers. The visual observations are consistent with the numerical solutions.

Keywords: Taylor vortices; annulus end effects; subcritical vortices; eccentric cylinders; anomalous circulation

Introduction

The flow between a rotating inner cylinder and a stationary outer cylinder, both concentric and eccentric, becomes centrifugally unstable at a sufficiently high rotational speed. More precisely, instability occurs when the critical value, T_c, of the Taylor number, T, is exceeded. The Taylor number is defined as

$$T=\frac{2\Omega_1^2 R_1^2 d^3}{\nu^2(R_1+R_2)}$$

and represents the ratio of centrifugal to viscous forces. The result of this instability is the appearance of contra-rotating toroidal vortices, known as Taylor vortices, superimposed on the basic flow.

Theoretical predictions of T_c assume the annulus to be infinitely long, while experimental rigs are necessarily finite. Experimental determination is usually by flow visualization or by torque measurement, the appearance of Taylor vortices causing a sharp increase in the slope of the torque–speed curve. Many flow visualization studies have observed the presence of vortex motions at Taylor numbers considerably less than the theoretically predicted value of T_c. Using aluminum paint pigment for flow visualization, Jackson, Robati, and Mobbs[1] detected weak vortex motions between concentric cylinders at $0.3T_c$ in an apparatus with a radius ratio of 0.908 and a length/gap ratio of 65. A sequence of different vortex motions occurred between $0.3T_c$ and T_c. A similar observation was made by Castle and Mobbs[2] for eccentric cylinders having a radius ratio of 0.9 and a length/gap ratio of 100, using dye injection. Vortex systems appeared at values of T well below T_c. The initial vortices were replaced by vortex cells of shorter axial length close to the expected value of T_c. Mobbs and Ozogan[3] have shown that subcritical vortex motions have a considerable effect on torque, measured on the outer cylinder, at the higher end of the subcritical Taylor number range. At high eccentricity ratios, this effect is sufficient to make the usual sharp increase in torque–speed slope at T_c undetectable (see, e.g., Vohr[4]).

In order to determine whether subcritical vortices are the result of annulus and effects, Preston[5] obtained numerical solutions to the flow equations for concentric cylinders, where the annulus length was determined by stationary end plates. His results showed the presence of vortex motions at low subcritical values of T, with the strongest vortex cells adjacent to the end plates. Similar numerical results have been obtained by De Roquefort and Grillaud[6] in the case of end plates rotating with the inner cylinder.

The current investigation extends the numerical work of Preston for concentric cylinders and also covers numerical solutions of the flow equations for eccentric cylinders with stationary annulus end plates.

Basic equations

For a steady, incompressible, isoviscous flow, the equations of motion and continuity are

$$\nabla(\tfrac{1}{2}\mathbf{q}^2)-\mathbf{q}\times(\nabla\times\mathbf{q})=-\frac{1}{\rho}\nabla p+\nu[\nabla(\nabla\cdot\mathbf{q})-\nabla\times\nabla\times\mathbf{q}] \quad (1)$$

and

$$\nabla\cdot\mathbf{q}=0 \quad (2)$$

The boundary conditions for the velocities are the same in both concentric and eccentric cases. All the velocity components are zero at both cylinders except for the azimuthal component at the inner cylinder, which is equal to the inner cylinder surface speed.

To eliminate the pressure term from Equation 1, two methods can be employed. The first involves the introduction of a stream function that satisfies the equation of continuity. The second method is the introduction of vorticity. Vorticity, $\omega(\xi,\eta,\zeta)$, is defined as:

$$\omega=\nabla\times\mathbf{q} \quad (3)$$

Taking the curl of Equation 1 causes the pressure term to

Address reprint requests to Dr. El-Dujaily at the Mathematics and Statistics Department, Polytechnic South West, Plymouth PL4 8AA, UK.

Received 27 February 1989; accepted 24 July 1989

disappear. Taking the curl of Equation 3 then gives—in component form—six equations with six unknowns. This method has proved to be more successful in three-dimensional problems, where a stream function cannot be used (see, e.g., Dennis *et al.*[7]).

When the cylinders are concentric, either method can be used. The governing equations in cylindrical polar coordinates and nondimensional form, using the first method, are

$$A\frac{\partial\psi}{\partial z}\left[\frac{\partial^3\psi}{\partial r^3}-\frac{2}{r^2}\frac{\partial\psi}{\partial r}+\frac{4\psi}{r^3}\right]+A^3\frac{\partial\psi}{\partial z}\left[\frac{\partial^3\psi}{\partial r\,\partial z^2}-\frac{1}{r}\frac{\partial^2\psi}{\partial z^2}\right]$$
$$-A\left[\frac{\partial\psi}{\partial r}+\frac{\psi}{r}\right]\left[\frac{\partial^3\psi}{\partial r^2\,\partial z}+\frac{1}{r}\frac{\partial^2\psi}{\partial r\,\partial z}\right]-A^3\left[\frac{\partial\psi}{\partial r}+\frac{\psi}{r}\right]\frac{\partial^3\psi}{\partial z^3}-\frac{2Av}{r}\frac{\partial v}{\partial z}$$
$$+\frac{1}{\mathrm{Re}}\left[\frac{\partial^4\psi}{\partial r^4}+\frac{2}{r}\frac{\partial^3\psi}{\partial r^3}-\frac{3}{r^2}\frac{\partial^2\psi}{\partial r^2}+\frac{3}{r^3}\frac{\partial\psi}{\partial r}-\frac{3\psi}{r^4}\right]$$
$$+\frac{2A^2}{\mathrm{Re}}\left[\frac{\partial^4\psi}{\partial r^2\,\partial z^2}+\frac{1}{r}\frac{\partial^3\psi}{\partial r\,\partial z^2}-\frac{1}{r^2}\frac{\partial^2\psi}{\partial z^2}+\frac{A^4}{\mathrm{Re}}\frac{\partial^4\psi}{\partial z^4}\right]=0 \tag{4a}$$

and

$$A\left[\frac{\partial\psi}{\partial r}+\frac{\psi}{r}\right]\frac{\partial v}{\partial z}-A\left[\frac{\partial v}{\partial r}+\frac{v}{r}\right]\frac{\partial\psi}{\partial z}-\frac{1}{\mathrm{Re}}\left[\frac{\partial^2 v}{\partial r^2}+\frac{1}{r}\frac{\partial v}{\partial r}-\frac{v}{r^2}\right]$$
$$-\frac{A^2}{\mathrm{Re}}\frac{\partial^2 v}{\partial z^2}=0 \tag{4b}$$

Where the Reynolds number $\mathrm{Re}=\Omega_1 d^2/\nu$ and the gap/length ratio $A=d/l$. The stream function is $\psi(r, z)$, such that

$$u=-\frac{1}{r}\frac{\partial(r\psi)}{\partial z},\quad \text{and}\quad w=\frac{1}{r}\frac{\partial(r\psi)}{\partial r} \tag{5}$$

and u, v, and w are the velocity components in the r, θ, and z directions, respectively.

The boundary conditions are

$$r=R_1;\qquad v=\frac{\eta'}{1-\eta'},\qquad \frac{\partial\psi}{\partial r}+\frac{\psi}{r}=0$$

$$r=R_2;\qquad v=0,\qquad \frac{\partial\psi}{\partial r}+\frac{\psi}{r}=0$$

and

$$z=0\quad\text{and}\quad z=l;\qquad v=0,\qquad \frac{\partial\psi}{\partial z}=0$$

where η' is the radius ratio R_1/R_2.

Using the vorticity–momentum method, we obtain the following governing equations:

$$\frac{\partial^2\xi}{\partial r^2}+\frac{\partial^2\xi}{\partial z^2}+\frac{1}{r}\frac{\partial\xi}{\partial r}-\frac{\xi}{r^2}=\mathrm{Re}\left\{u\frac{\partial\xi}{\partial r}+w\frac{\partial\xi}{\partial z}-\xi\frac{\partial u}{\partial r}-\zeta\frac{\partial w}{\partial z}\right\} \tag{6a}$$

$$\frac{\partial^2\eta}{\partial r^2}+\frac{\partial^2\eta}{\partial z^2}+\frac{1}{r}\frac{\partial\eta}{\partial r}-\frac{\eta}{r^2}=\mathrm{Re}\left\{u\frac{\partial\eta}{\partial r}+w\frac{\partial\eta}{\partial z}+\frac{v\xi}{r}-\xi\frac{\partial v}{\partial r}-\zeta\frac{\partial v}{\partial z}-\frac{\eta u}{r}\right\} \tag{6b}$$

$$\frac{\partial^2\zeta}{\partial r^2}+\frac{\partial^2\zeta}{\partial z^2}+\frac{1}{r}\frac{\partial\zeta}{\partial r}=\mathrm{Re}\left\{u\frac{\partial\zeta}{\partial r}+w\frac{\partial\zeta}{\partial z}-\xi\frac{\partial w}{\partial r}-\zeta\frac{\partial w}{\partial z}\right\} \tag{6c}$$

$$\frac{\partial^2 u}{\partial r^2}+\frac{\partial^2 u}{\partial z^2}+\frac{1}{r}\frac{\partial u}{\partial r}-\frac{u}{r^2}=\frac{\partial\eta}{\partial z} \tag{7a}$$

$$\frac{\partial^2 v}{\partial r^2}+\frac{\partial^2 v}{\partial z^2}+\frac{1}{r}\frac{\partial v}{\partial r}-\frac{v}{r^2}=\frac{\partial\zeta}{\partial r}-\frac{\partial\xi}{\partial z} \tag{7b}$$

and

$$\frac{\partial^2 w}{\partial r^2}+\frac{\partial^2 w}{\partial z^2}+\frac{1}{r}\frac{\partial w}{\partial r}=-\frac{1}{r}\frac{\partial}{\partial r}(r\eta) \tag{7c}$$

The vorticity components are given by

$$\xi=-\frac{\partial v}{\partial z},\qquad \eta=\frac{\partial u}{\partial z}-\frac{\partial w}{\partial r},\quad\text{and}\quad \zeta=\frac{1}{r}\frac{\partial}{\partial r}(rv)$$

The boundary conditions are

$$r=R_1;\qquad u=w=0,\qquad v=\frac{\eta'}{1-\eta'},\qquad \xi=0,\qquad \eta=-\frac{\partial w}{\partial r},$$
$$\zeta=\frac{1}{r}\frac{\partial}{\partial r}(rv)$$

$$r=R_2;\qquad u=v=w=0,\qquad \xi=0,\qquad \eta=-\frac{\partial w}{\partial r},\qquad \zeta=\frac{\partial v}{\partial r}$$

$$z=0\quad\text{and}\quad z=l;$$

Notation

- A Annulus gap/length ratio
- a Distance from O to P in bipolar coordinate system (Figure 1)
- A' Center of inner cylinder in bipolar coordinate system
- B' Center of outer cylinder in bipolar coordinate system
- C_r Clearance ratio
- d Gap between cylinders when concentric
- h Lamé coefficient
- l Annulus length
- p Pressure
- $\mathbf{q}$ Velocity vector
- Re Reynolds number
- R_1 Inner cylinder radius
- R_2 Outer cylinder radius
- r Radial coordinate
- T Taylor number
- T_c Critical Taylor number
- u Radial velocity
- v Tangential velocity
- w Axial velocity
- z Axial coordinate

Greek letters

- α Bipolar coordinate (Figure 1)
- α_1 Circle corresponding to inner cylinder in bipolar coordinate system
- α_2 Circle corresponding to outer cylinder in bipolar coordinate system
- β Bipolar coordinate (Figure 1)
- ε Eccentricity ratio
- η Radial vorticity component
- η' Radius ratio, R_1/R_2
- θ Tangential coordinate
- ζ Tangential vorticity component
- ξ Axial vorticity component
- ρ Fluid density
- ν Kinematic viscosity
- ψ Stream function
- Ω_1 Inner cylinder rotational speed
- ω Vorticity vector

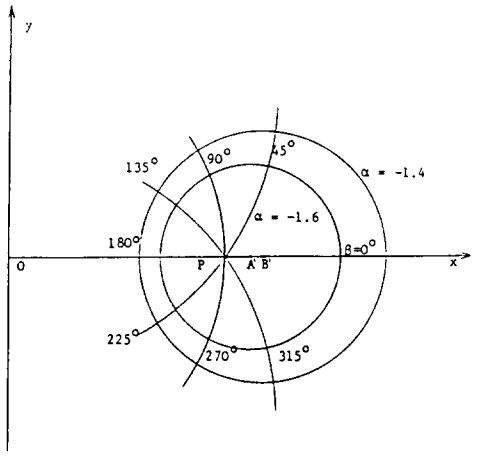

Figure 1 The bipolar coordinate system; $C_r=0.25$ and $\varepsilon=0.42$

and

$$u=v=w=0; \qquad \xi=-\frac{\partial v}{\partial z}, \qquad \eta=\frac{\partial u}{\partial z}, \qquad \zeta=0$$

When the cylinders are eccentric, the problem is a three-dimensional one and, hence, the vorticity–momentum method is used (Dennis *et al.*[7]). An appropriate coordinate system is the bipolar system used by Ritchie[8] in his analysis of the flow between infinitely long eccentric cylinders. The transformation from Cartesian coordinates (x, y, z) to bipolar coordinates (α, β, z) is given by

$$x=\frac{a\sinh\alpha}{\cosh\alpha-\cos\beta}, \qquad y=\frac{a\sin\beta}{\cosh\alpha-\cos\beta}, \quad \text{and} \quad z=z$$

where a is the distance from the Cartesian origin O to the pole P of the bipolar system (see Figure 1).

The Lamé coefficients are found to be $(h, h, 1)$, where

$$h=\frac{a}{\cosh\alpha-\cos\beta}$$

It follows, using the transformation, that

$$R_1=\frac{-a}{\sinh\alpha_1}, \quad \text{and} \quad R_2=\frac{-a}{\sinh\alpha_2}$$

$$C_r=\frac{R_2-R_1}{R_2}=\frac{\sinh\alpha_1-\sinh\alpha_2}{\sinh\alpha_1}$$

and

$$\varepsilon=\frac{OB'-OA'}{C}=\frac{\sinh(\alpha_1-\alpha_2)}{\sinh\alpha_1-\sinh\alpha_2}$$

Using this system of coordinates, we simply apply the boundary conditions:

$$\alpha=\alpha_1; \qquad u=w=0, \qquad v=\frac{\eta'}{1-\eta'}, \qquad \xi=0, \qquad \eta=-\frac{1}{h}\frac{\partial w}{\partial\alpha},$$

$$\zeta=\frac{1}{h^2}\frac{\partial}{\partial\alpha}(hv)$$

$$\alpha=\alpha_2; \qquad u=v=w=0, \qquad \xi=0, \qquad \eta=-\frac{1}{h}\frac{\partial w}{\partial\alpha},$$

$$\zeta=\frac{1}{h^2}\frac{\partial}{\partial\alpha}(hv)$$

and

$$z=0 \quad \text{and} \quad z=l; \qquad u=v=w=0, \qquad \xi=-\frac{\partial v}{\partial z}, \qquad \eta=\frac{\partial u}{\partial z},$$

$$\zeta=0$$

The governing equations for this case are

$$\frac{1}{h^2}\frac{\partial^2\xi}{\partial\alpha^2}+\frac{1}{h^2}\frac{\partial^2\xi}{\partial\beta^2}+\frac{\partial^2\xi}{\partial z^2}-\frac{(\cosh\alpha+\cos\beta)}{ah}\xi+\frac{2\sinh\alpha}{ah}\frac{\partial\eta}{\partial\beta}$$
$$-\frac{2\sin\beta}{ah}\frac{\partial\eta}{\partial\alpha}=\mathrm{Re}\left\{\frac{u}{h}\frac{\partial\xi}{\partial\alpha}+\frac{v}{h}\frac{\partial\xi}{\partial\beta}+w\frac{\partial\xi}{\partial z}+\frac{u\eta}{h^2}\frac{\partial h}{\partial\beta}-\frac{\xi}{h}\frac{\partial u}{\partial\alpha}\right.$$
$$\left.-\frac{\eta}{h}\frac{\partial u}{\partial\beta}-\zeta\frac{\partial u}{\partial z}-\frac{\xi v}{h^2}\frac{\partial h}{\partial\beta}\right\} \tag{8a}$$

$$\frac{1}{h^2}\frac{\partial^2\eta}{\partial\alpha^2}+\frac{1}{h^2}\frac{\partial^2\eta}{\partial\beta^2}+\frac{\partial^2\eta}{\partial z^2}-\frac{(\cosh\alpha+\cos\beta)}{ah}\eta-\frac{2\sinh\alpha}{\xi ah}\frac{\partial\xi}{\partial\beta}$$
$$+\frac{2\sin\beta}{ah}\frac{\partial\xi}{\partial\alpha}=\mathrm{Re}\left\{\frac{u}{h}\frac{\partial\eta}{\partial\alpha}+\frac{v}{h}\frac{\partial\eta}{\partial\beta}+w\frac{\partial\eta}{\partial z}+\frac{v\xi}{h^2}\frac{\partial h}{\partial\alpha}-\frac{\xi}{h}\frac{\partial v}{\partial\beta}\right.$$
$$\left.-\frac{\eta}{h}\frac{\partial v}{\partial\beta}-\zeta\frac{\partial v}{\partial z}-\frac{\eta u}{h^2}\frac{\partial h}{\partial\alpha}\right\} \tag{8b}$$

$$\frac{1}{h^2}\frac{\partial^2\zeta}{\partial\alpha^2}+\frac{1}{h^2}\frac{\partial^2\zeta}{\partial\beta^2}+\frac{\partial^2\zeta}{\partial z^2}$$
$$=\mathrm{Re}\left\{\frac{u}{h}\frac{\partial\zeta}{\partial\alpha}+\frac{v}{h}\frac{\partial\zeta}{\partial\beta}+w\frac{\partial\zeta}{\partial z}-\frac{\xi}{h}\frac{\partial w}{\partial\alpha}-\frac{\eta}{h}\frac{\partial w}{\partial\beta}-\zeta\frac{\partial w}{\partial z}\right\} \tag{8c}$$

$$\frac{1}{h^2}\frac{\partial^2u}{\partial\alpha^2}+\frac{1}{h^2}\frac{\partial^2u}{\partial\beta^2}+\frac{\partial^2u}{\partial z^2}-\frac{(\cosh\alpha+\cos\beta)}{ah}u+\frac{2\sinh\alpha}{ah}\frac{\partial v}{\partial\beta}-\frac{2\sin\beta}{ah}\frac{\partial v}{\partial\alpha}$$
$$=\frac{\partial\eta}{\partial z}-\frac{1}{h}\frac{\partial\zeta}{\partial\beta} \tag{9a}$$

$$\frac{1}{h^2}\frac{\partial^2v}{\partial\alpha^2}+\frac{1}{h^2}\frac{\partial^2v}{\partial\beta^2}+\frac{\partial^2v}{\partial z^2}-\frac{(\cosh\alpha+\cos\beta)}{ah}v-\frac{2\sinh\alpha}{ah}\frac{\partial u}{\partial\beta}+\frac{2\sin\beta}{ah}\frac{\partial u}{\partial\alpha}$$
$$=\frac{1}{h}\frac{\partial\zeta}{\partial\alpha}-\frac{\partial\xi}{\partial z} \tag{9b}$$

and

$$\frac{1}{h^2}\frac{\partial^2w}{\partial\alpha^2}+\frac{1}{h^2}\frac{\partial^2w}{\partial\beta^2}+\frac{\partial^2w}{\partial z^2}=\frac{1}{h}\frac{\partial\xi}{\partial\beta}+\frac{\xi}{h^2}\frac{\partial h}{\partial\beta}-\frac{1}{h}\frac{\partial\eta}{\partial\alpha}-\frac{\eta}{h^2}\frac{\partial h}{\partial\alpha} \tag{9c}$$

Method of solution

Because the boundary conditions at $z=0$ and $z=l$ are the same, we can assume that the solution will be symmetrical about the half-annulus plane. Therefore further boundary conditions at $z=l/2$ can be deduced, i.e.,

$$\frac{\partial u}{\partial z}=\frac{\partial v}{\partial z}=w=0$$

and

$$\frac{\partial\psi}{\partial z^2}=0, \qquad \xi=\eta=\frac{\partial\zeta}{\partial z}=0$$

Equations 4 and 6–9 can be written in finite-difference form using central differencing. The Gauss–Seidel iterative technique was used in solving the finite-difference form of the vorticity–momentum equations. The Newton–Raphson technique was applied to Equations 4, and the Gauss–Seidel technique was then employed to solve for the increment vector resulting from the application of the former method.

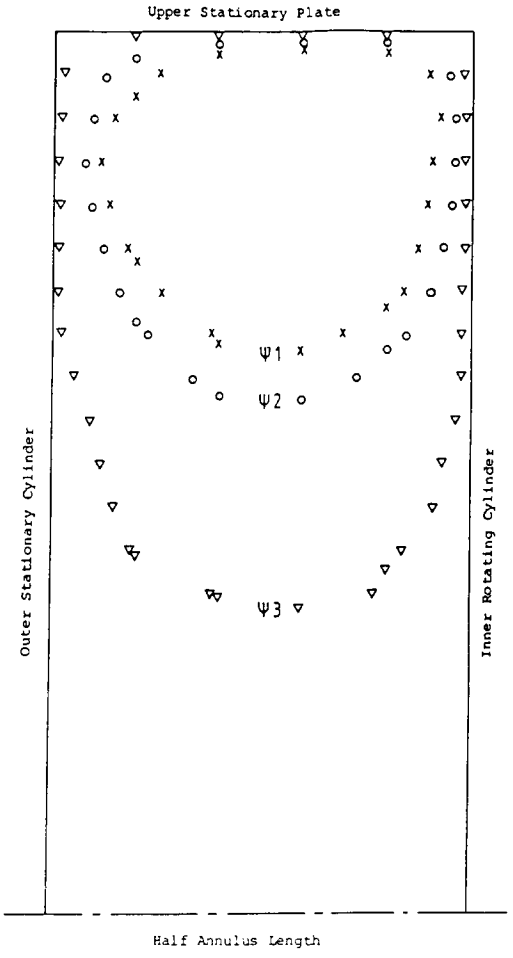

Figure 2a Subcritical vortex formation; $T/T_c = 0.01$, gap/length ratio $= 0.125$, radius ratio $= 0.9$, and 2 cells; values of stream function: $\psi_1 = -0.001313$, $\psi_2 = -0.000788$, and $\psi_3 = -0.0000263$

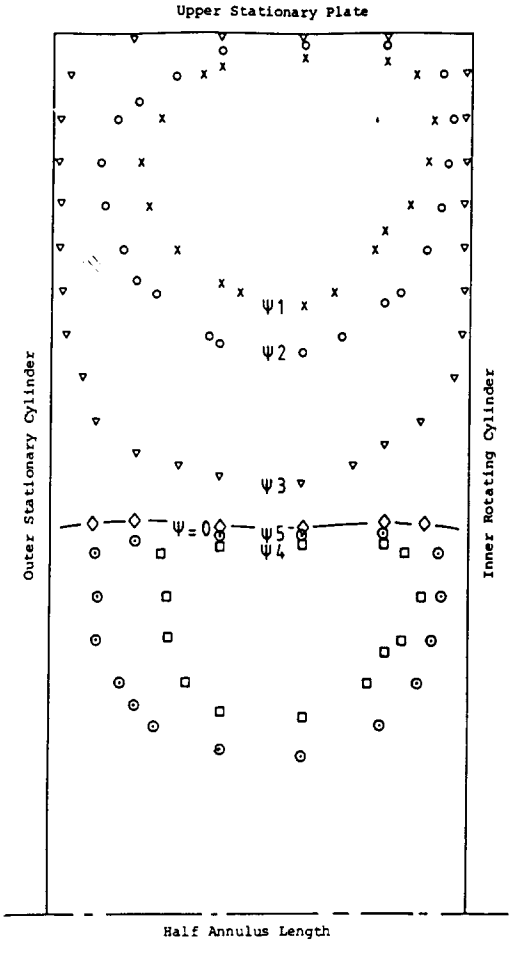

Figure 2b Subcritical vortex formation; $T/T_c = 0.1$ and 4 cells; values of stream function: $\psi_1 = -0.00860$, $\psi_2 = -0.00430$, $\psi_3 = -0.000258$, $\psi_4 = 0.000022$, and $\psi_5 = 0.000011$

The boundary conditions for Equations 4a and 4b are simply applied even when first-order derivatives are needed on solid boundaries. The reason is that sufficient information is available to allow the use of nodal points, one mesh size beyond the boundaries, i.e., outside the solution space.

The boundary conditions for the vorticity derivatives are not so simple to apply at solid boundaries. The information available is not sufficient to allow the use of nodal points outside the solution space. The boundary conditions for the first-order derivatives of the vorticities were therefore derived from the Taylor expansion series at nodal points one step and two steps away from the boundaries. An underrelaxation factor was necessary in the application of these boundary conditions.

The matrices associated with the finite-difference form of Equations 7 and 9 are diagonally dominant, whereas those associated with Equations 6 and 8 may not be. Therefore an underrelaxation factor is used in solving Equations 6 and 8, whereas an overrelaxation factor may be used in solving Equations 7 and 9 to speed the convergence.

Numerical analysis results

The numerical solutions obtained for the concentric cylinder problem, employing the stream function, were for a radius ratio of 0.9, a Taylor number ratio T/T_c of from 0.01 to 1.1, and aspect ratios of from 2 to 8. A typical streamline pattern in the r-z plane is shown in Figure 2. The tangential velocity distribution on inward and outward flow vortex cell boundaries are shown in Figure 3. The variation of number of vortex cells (i.e., the number of vortex cells in the flow domain) with the aspect ratio and Taylor number ratio T/T_c is presented in Figure 4. Solutions for concentric cylinders obtained using the vorticity–momentum equations were for radius ratios of 0.8 and 0.9, T/T_c ratios of from 0.1 to 0.3, and aspect ratios of from 2 to 8. A comparison between the results obtained by this method and those obtained by the former shows a similar variation in the number of cells with increasing Taylor number, only slightly slower when the radius ratio $= 0.8$. This is not surprising, as the value of the Reynolds number for a given T/T_c is smaller. Hence in Figure 5 we used the Reynolds number rather than T/T_c to allow for the difference in the radius ratio.

The numerical solutions obtained for the eccentric cylinder problem were for a radius of 0.8, T/T_c ratios of 0.1 and 0.2, aspect ratios of 2 to 6, and eccentricity ratios of 0.2 and 0.5. A solution was obtained for an eccentricity ratio of 0.001 to compare it with the concentric cylinder results.

The results are presented by plotting the radial and axial velocity components for some selected planes. In any vertical plane the maximum velocity component is represented by 0.9 of the distance between two adjacent mesh points. All other velocities in that plane are then normalized with respect to this maximum velocity. The distribution of radial velocity in the r-θ plane at the mid-point of the annulus length is given in

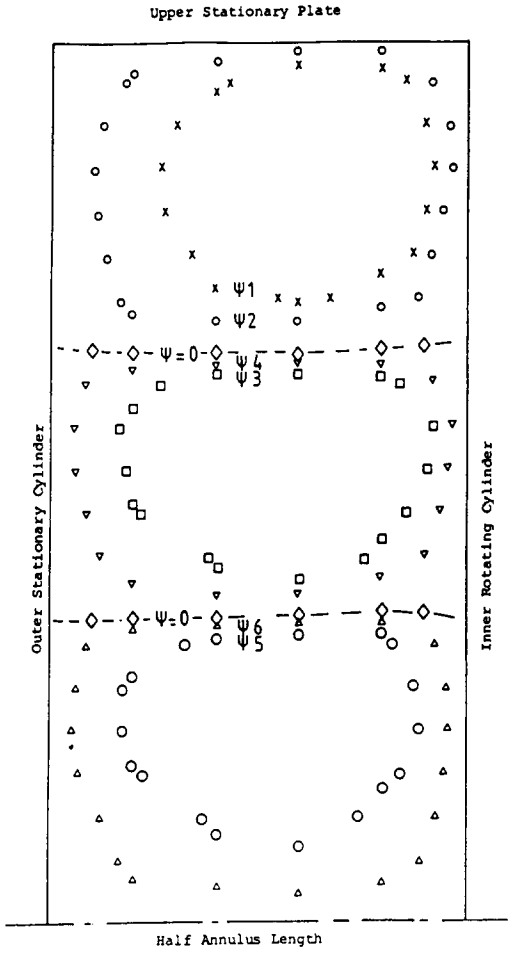

Figure 2c Subcritical vortex formation; $T/T_c = 0.6$ and 6 cells; values of stream function: $\psi_1 = -0.026216$, $\psi_2 = -0.008456$, $\psi_3 = 0.005920$, $\psi_4 = 0.001776$, $\psi_5 = -0.001326$, and $\psi_6 = -0.000398$

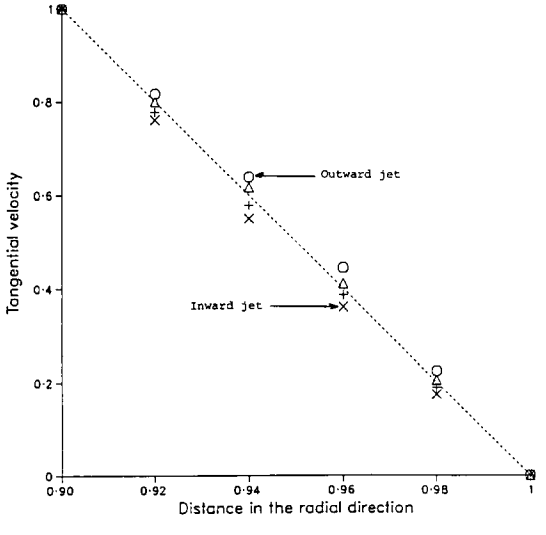

Figure 3 Tangential velocity distributions on vortex cell boundaries; $T/T_c = 0.6$, gap/length ratio = 0.2, radius ratio = 0.9, and 4 cells

Figure 6. The radial velocities are plotted in the circumferential direction with positive values in the same direction as the rotation of the inner cylinder, which is counterclockwise.

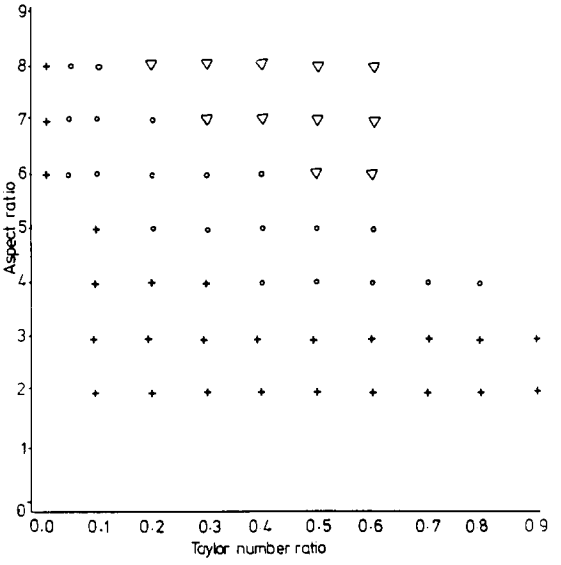

Figure 4 Vortex cell number as a function of aspect ratio (l/d) and Taylor number ratio (T/T_c) for concentric cylinders; stream function method; radius ratio = 0.9; 2 cells, +; 4 cells, ○; 6 cells, ▽

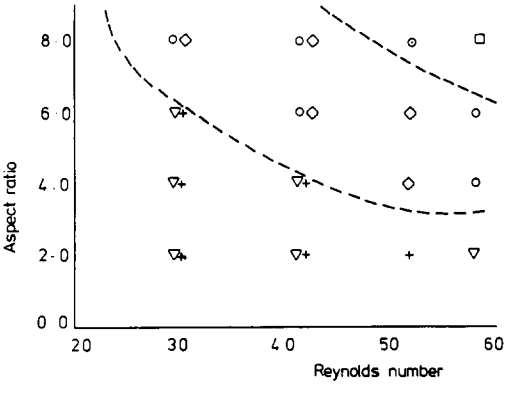

Figure 5 Comparison of the results of Figure 4 with those obtained using the vorticity–momentum equations; 2 cells, v–m +, sf ▽; 4 cells, v–m ◇, sf ○; 6 cells, v–m ⊙, sf □

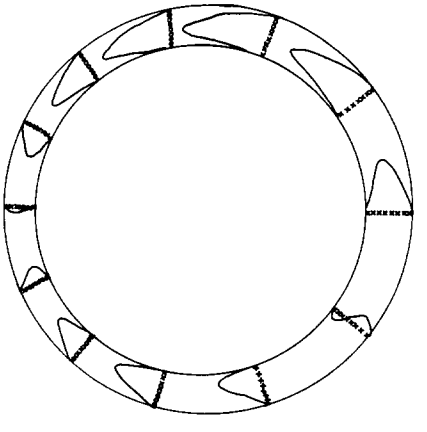

Figure 6 Radial velocity distribution in the mid-annulus plane for eccentric cylinders; counterclockwise is positive; inner cylinder is rotating counterclockwise; $T/T_c = 0.1$, radius ratio = 0.8, eccentricity ratio = 0.2, and aspect ratio = 4

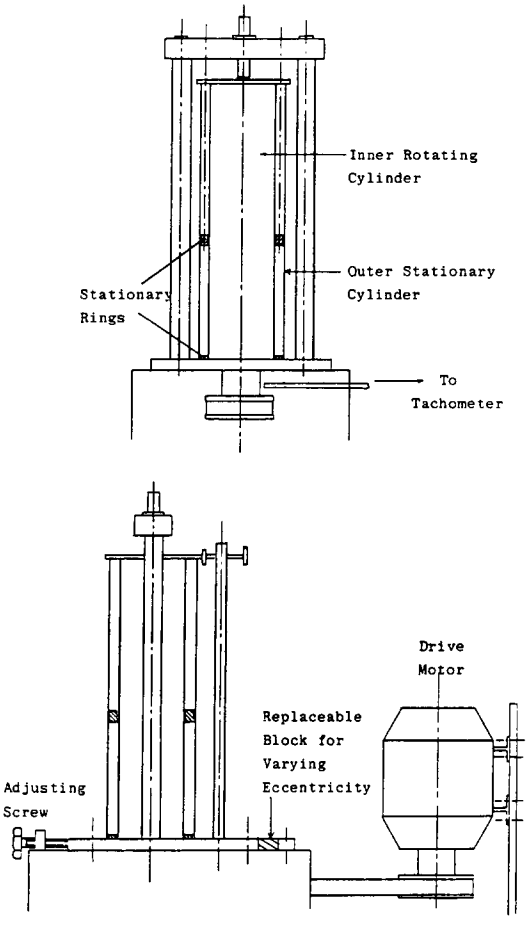

Figure 7 Schematic diagram of experimental rig B

Experimental investigation

Subcritical vortex motion—and sometimes supercritical Taylor vortex flow—were studied visually by the addition of aluminum flakes to the fluid. The annulus length was defined by two axially adjustable rings. These rings and the outer cylinder were stationary, and the inner cylinder rotated. Experiments were conducted on concentric cylinders with radius ratios of 0.8 and 0.9 and on eccentric cylinders with a radius ratio of 0.8 and eccentricity ratios of 0.2 and 0.5. The annulus aspect ratio was varied by moving the rings axially. Two rigs were used for these experiments. Rig A has an aluminum shaft of diameter 57.15 mm and length 203.2 mm. The outer cylinder is made of perspex and has a bore diameter of 63.5 mm. Rig B has an aluminum shaft of diameter 72 mm and length 305 mm. The outer cylinder is made of glass and has a mean bore diameter of 89.39 mm. Rig B has a facility of eccentric operation. Figure 7 presents a schematic diagram of rig B.

The experiments at a radius ratio of 0.9 had the aim of counting the number of cells in the subcritical region. The results of these experiments are compared with those of Figure 4 in Figure 8.

The experiments conducted on the rig with cylinders of radius ratio 0.8 examined the subcritical cell structure when the cylinders were both concentric and eccentric. The vortex activity was found to evolve in a manner similar to that depicted by the numerical analyses. For example, at a radius ratio of 0.8, an aspect ratio of 6, and $T/T_c = 0.8$ the end cell is 1.3 times longer than the adjacent cell, and at $T/T_c = 0.86$ the end cell is 1.2 times longer.

Discussion

The numerical results for the concentric cylinder case show that subcritical vortices are present at very low Taylor numbers. Initially, the number of vortices is two, which is true for all the aspect ratios investigated. As the Taylor number is increased, the number of subcritical vortices increases by the addition of vortex pairs. As the already existing cells become stronger, a pair of contra-rotating vortex cells evolve on either side of the mid-annulus plane. This evolution of cell pairs appears to continue until the number of cells equals the greatest even integer equal to or less than the aspect ratio (Figures 2a–2c). The center of circulation of the subcritical cells is close to the inner cylinder and, in the case of the end cells, is close to the ends. In all cases the direction of circulation in the end cells is such that there is an inward radial flow near the end plates. This flow appears to be governed by a positive radial pressure gradient set up in the tangential flow away from the ends. The tangential velocity distributions deviate from the predicted distributions for infinitely long cylinders as the Taylor number is increased. When the cylinders are short, the tangential velocity gradients increase near the inner and outer cylinders at Taylor numbers below the critical. This accounts for the appreciable effect of subcritical vortices on the torque observed by Mobbs and Ozogan.[3]

In the eccentric cylinder case, the subcritical vortices evolve similarly. The solution obtained for the special case of eccentricity ratio $\varepsilon = 0.001$ is in very good agreement with those obtained for the concentric cylinders problem. When the eccentricity ratio is increased to 0.2 and 0.5, while keeping all other variables constant, the solution ceases to be azimuthally symmetric. In fact, the cells change their direction of circulation over a considerable part of the region where the flow is diverging (Figure 6). For an eccentricity ratio of 0.2, this reverse or

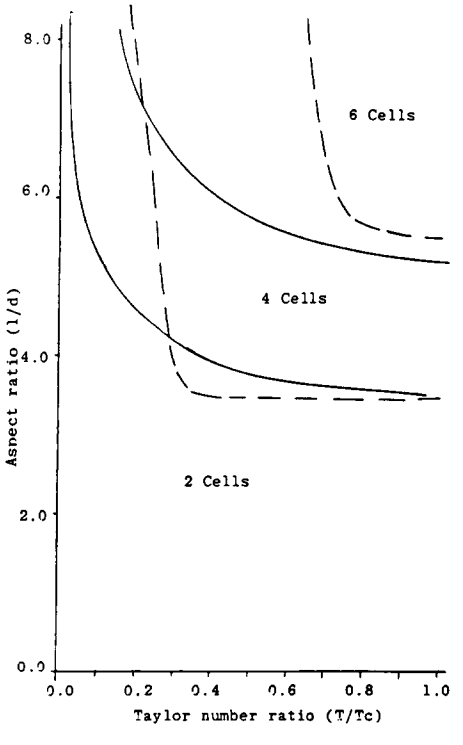

Figure 8 Comparison of vortex cell numbers in Figure 4 with those obtained experimentally; —— cell number boundaries as indicated by numerical results; ----- cell number boundaries as indicated by experimental results

anomalous circulation appears some distance upstream of the narrowest gap, being initially confined to a region near the inner cylinder. The normal circulation reappears some distance upstream of the widest gap in a region close to the outer cylinder. Increasing the Taylor number or the aspect ratio causes the changeover points to move closer to the narrowest and widest gaps, respectively.

Benjamin and Mullin[9] have observed many cases of Taylor vortex flow for concentric cylinders in which the direction of vortex circulation was anomalous. Visual observations of subcritical vortices in the flow between eccentric cylinders by Castle and Mobbs[2] showed the presence, at the widest gap, of vortices near the inner cylinder, which did not extend to the outer cylinder. This condition implies the existence of contra-rotating vortices near the outer cylinder in keeping with the numerical solution.

The numerical results for eccentric cylinders show the subcritical vortices to have their strongest circulation at an angle of between 30° to 60° downstream from the widest gap. An interesting comparison is with the predictions of the nonlocal stability theory of DiPrima and Stuart,[10] which show a maximum supercritical Taylor vortex activity at about 50° downstream from the widest gap.

The experiments confirm the results of the numerical analyses. Initially, at a sufficiently low Taylor number, there are two vortex cells, symmetric about the half-annulus plane, with their cores close to the end plates. This condition is true at all aspect ratios. As the Taylor number is increased, further pairs of cells evolve successively at the mid-annulus plane until the number of cells is generally equal to the aspect ratio. The results presented in Figure 8 show that in the experiments new cells appear to evolve at higher values of T/T_c than predicted by the numerical solutions. The reason probably is that in the newly developed cells the circulatory motion is very weak. When the Taylor number is increased, these cells become more vigorous and eventually become sufficiently strong to be visually detected. The results of the experiments on the eccentric cylinders show that the center of circulation of the end cells tends to be near the corner between the inner cylinder and the end plate. Other cells in the annulus tend to have their centers near the inner cylinder. The changes in the axial length of the cells are similar in nature to the concentric cylinder case, except that the dependence here is on the average gap width rather than the local gap width. The phenomenon of anomalous circulation of the cells in the diverging region of the flow could not be confirmed experimentally because the circulation was too weak to determine its direction.

References

1 Jackson, P.A., Robati, B., and Mobbs, F. R. Secondary flows between eccentric rotating cylinders at sub-critical Taylor numbers. Presented at the second Leeds–Lyon Symposium on Superlaminar Flow in Journal Bearings, 1975

2 Castle, P. and Mobbs, F. R. Hydrodynamic stability of the flow between eccentric cylinders, visual observations and torque measurements. *Proc. Inst. Mech. Eng.* 1968, **182**, 41–52

3 Mobbs, F. R. and Ozogan, M. S. Study of sub-critical Taylor vortex flow between eccentric rotating cylinders by torque measurements and visual observations. *Int. J. Heat and Fluid Flow*, 1984, **5**, 251–253

4 Vohr, G. H. An experimental study of Taylor vortices and turbulence in the flow between eccentric rotating cylinders. *J. Lub. Tech., Trans. ASME.* 1968, **90**, 275–296

5 Preston, W. S. A study of the sub-critical and wavy vortex regimes in the flow between concentric rotating cylinders. Ph.D. Thesis, University of Leeds, 1979

6 De Roquefort, T. A. and Grillaud, D. Computation on Taylor vortex flow by transient implicit method. *Comp. Fluid* 1978, **6**, 259–269

7 Dennis, S. C. R., Ingham, D. B., and Cook, R. N. Finite difference methods for calculating steady incompressible flows in three dimensions. *J. Comp. Phys.* 1979, **33**, 325–339

8 Ritchie, G. S. On the stability of viscous flow between eccentric rotating cylinders. *J. Fluid Mech.* 1968, **31**, 131–144

9 Benjamin, T. B. and Mullin, T. Notes on the multiplicity of flows in the Taylor experiment. *J. Fluid Mech.* 1982, **121**, 219–230

10 DiPrima, R. C. and Stuart, J. T. Non-local effects in the stability of flow between eccentric rotating cylinders. *J. Fluid Mech.* 1975, **67**, 85–111